



Targeting Vascular Cross Compression of Cranial nerves by MRI: Comparing different techniques for the diagnosis, characterization, and identification of prognostic factors

Badr Eldin Mostafa*, MD, Maha HA Abdel Salam#, MD, Mohammed A. El Begermey*, MD Ali N El Makhzangui*, Ali Shalash MD^ and Ali SH Mosleh*

From The Otorhinology, Radiology# and Neurology^ Departments
Ain-Shams University Faculty of Medicine
Cairo - Egypt*

Abstract

Conclusion: Heavy T 2-weighted MRI 3D driven equilibrium (DRIVE) is superior to 3D bFFE sequence in detecting neurovascular compressions, depicting their pattern and evaluating nerve morphology.

Objective: Compare 3D driven equilibrium (DRIVE) and 3-dimensional (3D) balanced fast-field echo (bFFE) MRI in detecting, and characterizing neurovascular cross compression as regards cause, type and effect on the affected nerve.

Patients and Methods: Forty-eight patients with clinical suspicion of vascular loop compression syndromes underwent MRI scans. There were 29 patients with audiovestibular symptoms, 12 with hemifacial spasm, 6 with trigeminal neuralgia and 1 with glossopharyngeal neuralgia. The cause and pattern of compression were compared on 3D driven equilibrium (DRIVE) and 3D bFFE images. The mean diameter of the involved nerve was compared to normal side. The MRI findings were compared to surgical findings in 42 cases.

Results: MRI outlined the conflict in 43/48 scanned patients (89.58%). 3D DRIVE revealed more anatomical details and more insulting vessels than 3D bFFE sequence ($p < 0.05$). As regards the offending vessel the concordance of MRI with surgical findings was 38/42 (84.4%). There was strong correlation ($p < 0.001$) between pre-operative MRI findings and intra-operative findings regarding the type of VCC, and nerve affection.

Keywords: neurovascular cross compression, 3D DRIVE MRI, 3D bFFE MRI, trigeminal neuralgia, hemifacial spasm, Retrosigmoid Microvascular decompression

Introduction

Neurovascular cross compression syndromes (NVCCS) are caused by pathological vascular contacts with different cranial nerves. Vascular compression of the cranial nerves in the cerebellopontine angle (CPA) can cause a number of functional disorders such as trigeminal neuralgia, hemifacial spasm, audiovestibular symptoms and glossopharyngeal neuralgia [1, 2, 3]. Microvascular decompression (MVD) has been established as the definitive treatment of NVC syndromes [1, 4, 5, 6]. Diagnosis is however one of exclusion in many cases and physicians and patients alike are skeptical. The radiological detection of a vessel in contact with a nerve may be a normal finding in up to 21% of asymptomatic persons [7]. Various radiological techniques can be used in a trial to delineate the offending vessel and the degree of compression. Currently, MRI is the most effective method for studying details of the brain stem, and surrounding vessels involved in NVC [8, 9, 10]. In this study we assessed the detectability of VCC using 3D driven equilibrium (DRIVE), and balanced fast-field echo (bFFE) MRI sequences and compare the demonstrated anatomical details aiming at precise identification, characterization of insulting vascular structure, the effect of compression on the affected nerve for the proper selection of patients who would benefit from MVD.

Patients and Methods

Between November 2006 and March 2009, 48 patients (27 males, and 21 females) aged 18-68 years (mean 45) were included in this study. Patients presented with signs and symptoms suggestive of NVCC. These included, hemifacial spasm, trigeminal neuralgia and various audiovestibular symptoms (unilateral tinnitus, unilateral SNHL, atypi-

cal and/or disabling positional vertigo). Patients were subjected to full medical history, clinical neurological and otorhinolaryngological examination and audio-vestibular assessment. Other possible pathologies were excluded a posteriori after investigations were completed. The study design was approved by the ethical committee of Ain-Shams University Faculty of Medicine and patients signed an informed consent for their participation in the study.

All patients underwent a high resolution CT scan with contrast followed by an MRI.

All MRI examinations were conducted using a 1.5 T (Intera; Philips Medical Systems, Best, The Netherlands). After completion of routine un-enhanced MR imaging of the brain, MR cisternography T2 weighted studies included: 3D DRIVE and 3D bFFE sequences. The parameters for DRIVE imaging included repetition time (TR), 1500 milliseconds; echo time (TE), 250 milliseconds; field of view, 13x13 cm; matrix size, 256x204; slice thickness, 0.7 mm; NSA, 2; and acquisition time, 4 minutes 32 seconds. The parameters for bFFE sequence were: TR, 15 milliseconds; TE, 7.5 milliseconds; field of view, 15x15 cm; flip angle, 50 degrees; matrix size, 256x190; slice thickness, 0.7 mm; NSA, 2; and acquisition time, 5 minute 47 seconds. Both MR sequences were acquired in the axial plane using a SENSE factor of 2. Both axial and coronal MR slices were reformatted.

The following anatomical structures were evaluated: cranial nerves, vascular anatomy at cerebellopontine angle (CPA) and vertebrobasilar (VB) arterial system, and offending VCC if present. The visualization of each structure was graded and scored:

- ◆ 1 (poor) if an anatomical structure was not visible,
- ◆ 2 (fair) visible anatomical structure with only minor artifacts,
- ◆ 3 (excellent) anatomical structure clearly visible with no artifacts.

Neurovascular cross-compression was deemed present if the nerve and the vessel were inseparable by an identifiable CSF cleft in two of three orthogonal planes.

The pattern of compression was characterized into 4 types: [11]

- ◆ Type 1 point compression where the implicated vessel compresses only a limited portion of the nerve,
- ◆ Type 2 longitudinal compression where both nerve and vessel are parallel,
- ◆ Type 3 loop compression where the vessel encircles the nerve,
- ◆ Type 4 indentation where the vessel indents the affected nerve.
- ◆ Finally, MR morphometric assessment of the involved nerve is carried out by comparing the mean diameter of the affected nerve to that of the contra-lateral healthy side.

Forty-five patients with suspected VCC underwent retrosigmoid endoscopic micro-vascular decompression. MRI findings were compared to intra-operative endoscopic findings in all cases as regarding: the presence and identification of the offending vessel, the type of the VCC and the morphology of the implicated nerve and the surrounding structures.

Statistical analysis

Statistical analysis was done on a personal computer using the Statistical Package for Social Sciences (SPSS[®]) version 17. Non-normally distributed numerical data were presented as median (range), and paired data were compared non-parametrically using Wilcoxon's signed ranks test. Correlation between nominal parameters was tested using Spearman's correlation test. A Spearman's correlation coefficient (rho) of 0.2-0.4 was regarded as denoting mild correlation, of 0.4-0.7 as denoting moderate correlation, of 0.7-1.0 as denoting strong correlation. At all instances, $p < 0.05$ was taken as denoting statistical significance.

Results

The study included 48 patients (27 males, and 21 females) aged 18-68y. There were 29 patients with audiovestibular symptoms, 12 with hemifacial spasm, 6 with trigeminal neuralgia and 1 with glossopharyngeal neuralgia. VCC was suspected on MRI in 43/48 patients. The visibility scores for all studied structures are depicted in Table 1.

Table 1: Comparison between visibility scores by 3DD and 3DbFFE

Visibility	3DD			3DbFFE			P value
	median	Minimum	maximum	median	Minimum	Maximum	
CNs	3	3	3	3	3	3	1.0
CPA vessel	3	3	3	3	2	3	0.014
VB vessel	3	3	3	3	3	3	1.0
VCC	3	2	3	3	1	3	0.006



As regards the VCC type, 39 cases could be evaluated (Table 2), the commonest being type 4, i.e. point compression of the vessel and nerve. (Figures 1, 2, 3, 4) Various offending vessels could be suspected by their anatomical course and location (Table 3). The commonest recognized vessel was the AICA (32 cases) (Figure 5). MRI could not differentiate the vascular nature of the offending vessels, whether arterial or venous.

Table 2: Type of NVCC on MRI

Type	Number (n = 39)	Percentage (%)
1	9	23
2	6	15
3	9	23
4	15	38

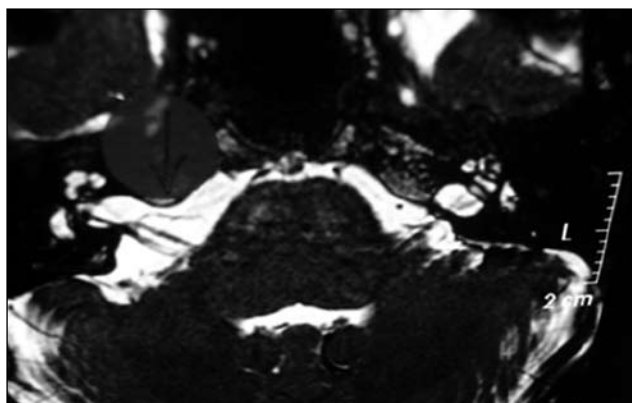


Figure 1: 3D bFFE showing a type 1 AICA loop

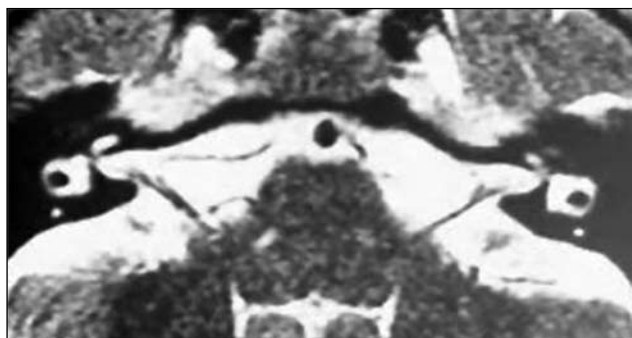


Figure 2: 3D bFFE showing a type 2 AICA loop

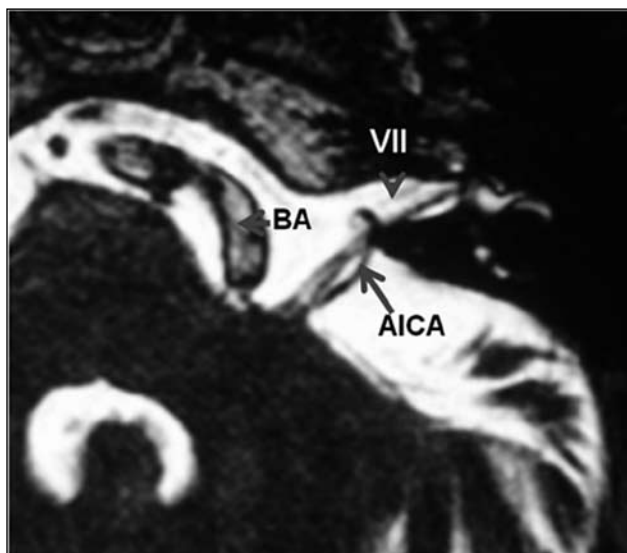


Figure 3: 3D DRIVE image showing a double conflict basilar artery (BA) and type 3 AICA loop

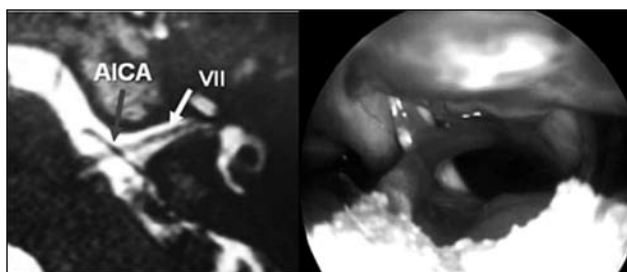


Figure 4:
A – 3D DRIVE image showing a type 4 conflict .
B – Endoscopic picture showing the AICA loop

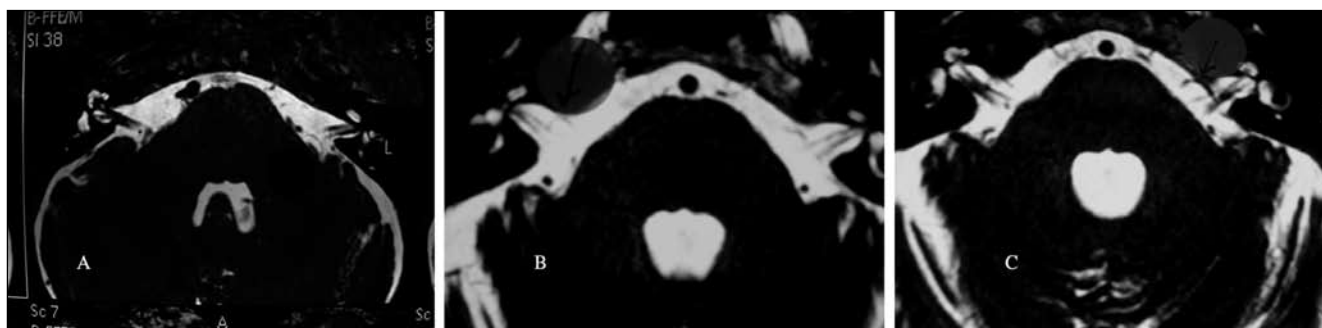


Figure 5: AICA loop comparison between different techniques:
A – Conventional MRI
B – 3D bFFE
C – 3D DRIVE showing the loop clearly (arrow)

Table 3: Offending vessels on MRI

Clinical picture	Number	Vessel	Number
TG Neuralgia	4	SCA	3
HFS	10	AICA	5
		VBA	4
		PICA	1
Vestibulocochlear	28	AICA	27
		PICA	1
Glossopharyngeal	1	PICA	1

As regards the affection of implicated nerve by MRI, 39 cases could be evaluated. Of these 27 [69.1%] nerves had a normal diameter while 12 nerves [30.9%] were thinner than the contralateral side.

Forty-five cases underwent retrosigmoid endoscopic microvascular decompression. Intra-operative findings as regards the offending vessels are summarized in Table 4. The concordance of MRI with surgical findings was 38/42 (84.4%) (Table 5). In 9 cases additional venous structures could be seen coursing along the vessel. In all cases thick arachnoid folds could be seen between the vessels and nerves. These could not be depicted on MRI. On the other hand, there was perfect correlation with VCC type revealed on surgical exploration ($\rho = 1.0$, $p < 0.001$) (table 6). As regards nerve morphometry there was a significant correlation between MRI and surgical findings (ρ) of 0.767 ($p < 0.001$).

Table 4: Intraoperative offending vessels

Endoscopic findings	Number	Clinical picture
AICA	5	HFS
VBA	3	
PICA	1	
Pontine Vein	1	
SCA	3	Trigeminal Neuralgia
Dandy's vein	2	
AICA	25	Vestibulocochlear
AICA (not compressing).	2	
PICA	1	
VBA	2	

Table 5: Comparison between the vessels identified on MRI and during surgery

Vessel	MRI	Surgery
Vestibulocochlear pathology		
	28	30
AICA	27	25
AICA not compressing		2
PICA	1	1
VBA		2
Hemifacial spasm		
	10	10
AICA	5	5
PICA	1	1
VBA	4	3
Pontine vein		1
Trigeminal neuralgia		
	4	5
SCA	3	3
Dandy's vein		2

Table 6: Correlation between the suspected type of compression on MRI and during surgery

	Types	MRI				Total	
		4	3	2	1		
Surgery	4		15	0	0	0	15
		%	100				38.5
	3		0	9	0	0	9
		%		100			23.1
	2		0	0	6	0	6
		%			100		15.4
	1		0	0	0	9	9
		%				100	23.1
Spearman's correlation (ρ) = 1 ($p < 0.001$)							

Discussion

Before the availability of thin-slice MR imaging, vascular compression of cranial nerves in vivo had not been reported because it was very difficult to disclose neurovascular conflict by standard MR imaging or computed tomography. MR imaging with high-resolution 3D images is a highly sensitive method for revealing the details of the CPA and its neurovascular structures. Unlike 2D MRI, 3D MRI can provide volume imaging and ultra-thin slices. Basically, two

techniques denoted by various names are most widely used to provide high spatial resolution MR imaging of the temporal bone with a consistent cisternographic effect: 3D fast spin-echo (FSE) and 3D fast gradient-echo (FGRE) techniques. In clinical settings, the acquisition of these heavily T2-weighted images of good quality requires not only a high signal from the fluid-containing spaces and less of artifacts from motion and magnetic susceptibility, but also a short examination time [9, 10, 12]. Yet, both techniques bear



some inherent disadvantages including a relatively long scan time and inconsistent cisternographic effect [13]. As for 3D FGRE techniques, the inherent strong magnetic susceptibility effect may result in banding or zebra-stripe artifacts degrading the image quality [9,14]. Currently, 3D DRIVE and 3D bFFE sequences are considered as state-of-the-art imaging methods for MR cisternography [12, 13, 15]. 3D FSE sequences using FASE and DRIVE were superior to 3D FGRE using CISS and bFFE, respectively in evaluating the cranial nerves within IAC and the inner ear structures [9,14] but may show lasrge CSF artifacts [16]. On the other hand 3D bFFE was better than FSE sequences in demonstrating structures in and around the skull base without blurring and susceptibility artifacts due to less CSF pulsation artifacts [17].

In this study, 48 patients with clinical suspicion of vascular loop compression syndromes underwent MRI studies 3D DRIVE and 3D bFFE achieved comparable visibility of cranial nerves, vessels at CPA, and VB arterial system with $p > 0.05$ (statistically insignificant). CSF pulsations did not interfere with the visibility of cranial nerves and vessels on DRIVE, and bFFE sequences .

Regarding the visibility of vascular cross compression (VCC), this study depicted more offending VVC by 3D DRIVE than by bFFE MR sequence ($p < 0.01$). We found that on bFFE the signal intensities of the cranial nerves, vessels, and brain were similar, thus, it is difficult to clearly differentiate one structure from another. In addition, hyperintense susceptibility and flow artifacts rendered the detection of vessels more difficult. In contrast, on 3D DRIVE vessels are completely signal void, cranial nerves are of moderate low signal intensity and CSF is of profound high signal intensity. This allows proper identification of various structures.

High resolution MR sequences made it possible to analyze cranial nerves quantitatively for the first time

[18,19,20]. Quantitative MRI measurements allow a pathological neurovascular conflict to be differentiated from non pathological vessel-nerve proximity. In this study, we found reduced mean nerve diameter on the affected side in 12 cases (30.8%) having VCC that was confirmed by surgery.

Anatomical findings may affect the final outcome of MVD [20]. These include the type of compressing vessels, the severity of compression, the presence of nerve atrophy, and the presence of arachnoiditis. In this study, MRI examinations could characterize the severity of VCC and type of compression. There was a strong correlation between the pre-operative MRI findings and the endoscopic intra-operative findings ($p < 0.001$), regarding the site and type of VCC. This helps the pre-operative surgical planning and allows the surgeon to predict the possible outcome after surgery. However we could not differentiate between arteries and veins by MR sequences. The presence of associated arachnoiditis with or without nerve thinning could not be diagnosed by MRI

Conclusion

High-resolution heavy T2-weighted MR sequences including 3D DRIVE and bFFE with the SENSE technique are indispensable if VCC is suspected as they provide valuable information regarding the presence of VCC, anatomical type and severity of VCC, and the quantitative assessment of the implicated nerve. In this work, 3D DRIVE was superior to bFFE sequence as it depicted more anatomical details and diagnosed more VCC. Pre-operative MR evaluation using 3D Drive can evaluate prognostic anatomical factors regarding the severity of VCC and presence of affected nerve atrophy, thus helping selection of patients and improving surgical strategies as well as predicting the final prognosis for recovery.

References:

1. Badr-El-Dine M, El-Garem H, Talaat A, Magnan J. Endoscopically assisted minimally invasive Microvascular decompression of hemifacial spasm. *Otol Neurotol* 2002; 23: 122–128
2. Bayazit YA, Goksu N. Tinnitus and neurovascular compression. *ORL J Otorhinolaryngol Relat Spec.* 2008; 70(3): 209.
3. van der Steenstraten F, de Ru A J, Witkamp TD. Is Microvascular Compression of the Vestibulocochlear Nerve a Cause of Unilateral Hearing Loss? *Annals of Otolaryngology, Rhinology and Laryngology*, 2007 116(4): 248-252.
4. Miyazaki H, Deveze A, Magnan J. Neuro-otologic surgery through minimally invasive retrosigmoid approach: endoscope assisted microvascular decompression, vestibular neurectomy, and tumor removal. *Laryngoscope* 2005;115: 1612–161
5. Mostafa BE, El Sharnoubi M, Youssef AM. The keyhole retrosigmoid approach to the cerebello-pontine angle: indications, technical modifications, and results. *Skull Base.* 2008 Nov;18(6): 371-6
6. Goksu N, Bayazit YA, Bayramoglu I, Isik B, Yilmaz M, Kurtipek O, Uygur M. Surgical exposure in retrosigmoid approach: do we need cerebellar retractors? *Surg Neurol.* 2006;65: 631–634
7. De Carpentier J, Lynch N, Fisher A, et al. MR imaged neurovascular relationships at the cerebellopontine angle. *Clin Otolaryngol.* 1996; 21: 312-316.
8. Goh BT, Poon CY, Peck RH. The importance of routine magnetic imaging in trigeminal neuralgia diagnosis. *Oral Surg Med Oral Pathol Oral Radiol Endod.* 2001; 92(4): 424-429.



9. Naganawa S, Koshikawa T, Fukatsu H, et al. MR cisternography of the cerebellopontine angle: comparison of three-dimensional fast asymmetrical spin-echo and three-dimensional constructive interference in the steady-state sequences. *AJNR Am J Neuroradiol* 2001; 22: 1179-1185.
10. Nakashima K, Morikawa M, Ishimaru H, et al. Three-dimensional fast recovery fast spin-echo imaging of the inner ear and the vestibulocochlear nerve. *Eur Radiol* 2002; 12: 2776-2780.
11. Sirikci A., Bayazit Y., Ozer E., Ozkur A., Adaletli I., Cuce M. A. and Bayram M. (2005): Magnetic resonance imaging based classification of anatomic relationship between the cochleovestibular nerve and anterior inferior cerebellar artery in patients with non-specific neuro-otologic symptoms. *Surg Radiol Anat*, 27: 531-535.
12. Schmalbrock P. Comparison of three dimensional fast spin echo and gradient echo sequences for high-resolution temporal bone imaging. *J Magn Reson Imaging* 2000; 12: 814-825.
13. Melhem ER, Itoh R, Folkers PJ. Cervical spine: three-dimensional fast spin-echo MR imaging improved recovery of longitudinal magnetization with driven equilibrium pulse. *Radiology* 2001; 218: 283-288.
14. Yung NY, Moon WJ, Lee MH, et al. Magnetic resonance cisternography: comparison between 3-dimensional driven-equilibrium with sensitivity encoding and 3-dimensional balanced fast-field echo sequences with sensitivity encoding. *J Comput Assist Tomogr* 2007; 31: 588-591.
15. Ciftci E, Anik Y, Arslan A, et al. Driven equilibrium (DRIVE) MR imaging of the cranial nerves V-VIII: comparison with the T2-weighted 3D TSE sequence. *Eur J Radiol* 2004; 51: 234-240.
16. Tanrikulu L, Hastreiter P, Troescher-Weber R, et al. Intra-operative three-dimensional visualization in microvascular decompression. *J Neurosurg* 2007; 107: 1137-1143.
17. Tsuchiya K, Aoki C, Hachiya J. Evaluation of MR cisternography of the cerebellopontine angle using a balanced fast-field-echo sequence: preliminary findings. *Eur Radiol* 2004; 14: 239-242.
18. Kress B, Schindler M, Rasche D, et al. MRI volumetry for the pre-operative diagnosis of trigeminal neuralgia. *Eur Radiol* 2005; 15: 1344-1348.
19. Erbay SH, Bhadelia RA, O'Callaghan M, et al. Nerve atrophy in severe trigeminal neuralgia: non-invasive confirmation at MR imaging-initial experience. *Radiology* 2006; 238(2): 689-692.
20. Sindou M, Leston J, Decullier E, et al. Microvascular decompression for primary trigeminal neuralgia: long-term effectiveness and prognostic factors in a series of 362 consecutive patients with clear-cut neurovascular conflicts who underwent pure decompression. *J Neurosurg* 2007; 107: 1144-1153.

Corresponding Author:

Professor Badr E. Mostafa
48 Ibn El Nafees street
11371-Nasr City Cairo
EGYPT

Email: bemostafa@yahoo.com
bemostafa@med.asu.edu.eg

